Volume 43, Issue 8, 28 May 2010   ISSN 0021-9290

ELSEVIER

Journal of Biomechanics

Editor-in-Chief
Farshid Guilak

Shear wave induced resonance elastography of soft heterogeneous media

Anis Hadj Henni [a,*], Cédric Schmitt [a,b], Guy Cloutier [a,b,c,**]

[a] Laboratory of Biorheology and Medical Ultrasonics, University of Montreal Hospital Research Center (CRCHUM), Montreal, QC, Canada H2L 2W5
[b] Institute of Biomedical Engineering, University of Montreal, Montreal, QC, Canada H3C 3J7
[c] Department of Radiology, Radio-Oncology and Nuclear Medicine, University of Montreal, Montreal, QC, Canada H3T 1J4

ARTICLE INFO

ABSTRACT

In the context of ultrasound dynamic elastography imaging and characterization of venous thrombosis, we propose a method to induce mechanical resonance of confined soft heterogeneities embedded in homogenous media. Resonances are produced by the interaction of horizontally polarized shear (SH) waves with the mechanical heterogeneity. Due to such resonance phenomenon, which amplifies displacements up to 10 times compared to non-resonant condition, displacement images of the underlying structures are greatly contrasted allowing direct segmentation of the heterogeneity and a more precise measurement of displacements since the signal-to-noise ratio is enhanced. Coupled to an analytical model of wave scattering, the feasibility of shear wave induced resonance (SWIR) elastography to characterize the viscoelasticity of a mimicked venous thrombosis is demonstrated (with a maximum variability of 3% and 11% for elasticity and viscosity, respectively). More generally, the proposed method has the potential to characterize the viscoelastic properties of a variety of soft biological and industrial materials.

1. Introduction

Dynamic elastography is a medical imaging modality that provides a quantitative elasticity map of soft biological tissues (Eisencher et al., 1983; Krouskop et al., 1987; Parker and Lerner, 1992). Physically, it consists in generating low frequency shear waves (50–1000 Hz, typically) that propagate into the scanned medium. The elasticity map is obtained by imaging the shear wave propagation (i.e., tissue displacements or strains and wave velocity) and by using an adapted inverse problem. Dynamic elastography imaging aims to enhance the diagnosis of pathologies inducing local mechanical changes in organs like liver, breast, lung, etc. Elasticity imaging methods also have the potential to characterize the elasticity of vascular pathologies, like deep venous thrombosis (DVT), in order to enhance their medical diagnosis. Indeed, it is well known that the viscoelasticity of coagulated blood (Shah and Janmey, 1997, Evans et al., 2008) depends on its composition (Kaibara, 1996; Ryan et al., 1999) and age (Burghardt et al., 1995; Williams et al., 2006). Exploiting these dependences with static elastography methods has been shown feasible for assessing qualitatively elastic properties of DVTs (Emelianov et al., 2002; Rubin et al., 2003). But main limitations of these methods, contrary to dynamic approaches, are that the elasticity characterization is not quantitative, the viscosity is not assessed, and the mechanical behavior is highly dependant on the boundary conditions of the medium.

Different approaches exist to generate low frequency shear waves for dynamic elastography imaging of soft tissues. These methods employ external vibrating sources in contact with the structure to image (Parker et al., 1990; Muthupillai et al., 1995), or an internal excitation using ultrasound radiation force to generate shear waves deeply into tissues (Bercoff et al., 2004, Palmeri et al., 2005). These techniques are used in sonoelasticity, magnetic resonance elastography and transient ultrasound elastography to image, among other medical applications, confined pathologies like tumors. Paradoxically, except for vibro-acoustic spectrography (Fatemi and Greenleaf, 1998), which concerns vibration of hard tissues at high acoustical frequencies, the abovementioned excitation methods generally do not take advantage of the confined geometry of certain pathologies (Greenleaf et al., 2003). Inspired by the theory of elastic resonance excitation by wave scattering (Flax et al., 1978), shear wave induced resonance elastography (SWIR Elastography, SWIRE) consists in forcing the mechanical resonance of confined heterogeneities subjected to properly chosen incident shear waves. The aim of this development is twofold. The first objective is to improve the potential of dynamic elastography imaging to segment mechanically heterogeneous regions by maximizing the displacement contrast between the heterogeneity and its surrounding medium. The

* Corresponding author. Tel.: +1 514 890 8000 (24773); fax: +1 514 412 7505.
** Corresponding author at: Laboratory of Biorheology and Medical Ultrasonics, University of Montreal Hospital Research Center (CRCHUM), Montreal, QC, Canada H2L 2W5. Tel.: +1 514 890 8000 (24703); fax: +1 514 412 7505.

E-mail addresses: anis.hadjhenni@gmail.com (A.H. Henni),
guy.cloutier@umontreal.ca (G. Cloutier).

second objective is to propose a viscoelasticity characterization method based on the inclusion resonance properties.

With the objective to develop new methods to image and characterize viscoelasticity of deep vein thrombi (and of any equivalent structure) using dynamic elastography, shear wave induced resonance of a circular cylindrical heterogeneity is proposed. In a first time, and to solve the forward problem, SWIRE was studied theoretically and investigated experimentally in a phantom containing a circular cylindrical heterogeneity made of very soft material mimicking coagulated blood, as performed in a recent work using vertically polarized shear (SV) waves with no induction of resonance (Hadj Henni et al., 2008). In the present study, horizontally polarized shear (SH) waves, as used by Papazoglou et al. (2009), permitted to induce low frequency resonance of a soft heterogeneity. Theoretically, an analytical model (Morse and Feshbach, 1953; Biwa et al., 2004) to simulate the heterogeneity-shear wave interaction was implemented to predict the resonance frequencies and eigenmodes. Experimental and theoretical results (resonance spectra and eigenmode images) are compared to validate the modeling.

In a second time, this model served to formulate and solve an inverse problem in order to evaluate the feasibility of characterizing the viscoelasticity of two different soft and confined heterogeneities using SWIRE. Finally, the contribution of SWIRE to dynamic elastography imaging and viscoelasticity characterization is discussed.

2. Theoretical model

In order to understand theoretically the resonance phenomena of heterogeneities induced by shear waves and to explore their potential for dynamic elastography and soft material characterization, an analytical model was developed to simulate the scattering of a SH wave by a cylindrical circular heterogeneity embedded in a different material. Indeed, as it will be shown later, resonances are produced by the mechanism of scattering and refraction of SH waves as a result of the viscoelastic contrast existing between constituents of the propagation medium.

The harmonic plane incident shear wave propagated following the x direction (perpendicularly to the heterogeneity) and was polarized following the cylinder axis in the z direction (see Fig. 1). One can notice that these characteristics are those of a plane

SH-wave. Both materials were assumed to be homogeneous, isotropic and linear viscoelastic and since the displacement field is purely transverse, its divergence is equal to zero. In the frequency domain, by omitting the harmonic time dependence term $e^{i\omega t}$, the Navier differential equation, which governs the displacement field in the two media (Achenbach, 1973), becomes a Helmholtz equation

$$\mu_j(\Delta \mathbf{U}_j) + \rho_j \omega^2 \mathbf{U}_j = 0 \text{ with } j = \{1, 2\}, \tag{1}$$

where $\mathbf{U}_j = U_j \mathbf{e}_z$ is the stationary displacement field in medium j (j equals 1 for the heterogeneity material and 2 for the surrounding one), whereas ρ_j is the density of the current phase. In the following, the wave number in each phase is defined by $k_{T_j} = \omega / \sqrt{\mu_j / \rho_j}$. One has to note that the complex shear Lamé coefficients μ_j can have any arbitrary form. In other words, materials of media 1 and 2 can be governed by any viscoelastic behavior law like Kelvin–Voigt, Maxwell, Kelvin–Voigt fractional derivative, Zener, Jeffrey, etc.

The Helmholtz Eq. (1) can be solved in a cylindrical system of coordinates (o,$\mathbf{e}_r$, $\mathbf{e}_\theta$), see Fig. 1, by the mean of Bessel and trigonometric function series (Morse and Feshbach, 1953). Displacement field in medium 2 is a combination of the known incident plane wave and the scattered one. This latter and displacements within the inclusion (medium 1) are expressed using infinite series containing unknown coefficients A_n and B_n

$$U_1 = \sum_{n=0}^{+\infty} A_n J_n(k_{T_1} r) \cos(n\theta)$$

$$U_2 = \sum_{n=0}^{+\infty} (B_n H_n^{(1)}(k_{T_2} r) + \varphi(\omega)\varepsilon_n(i)^n J_n(k_{T_2} r)) \cos(n\theta) \tag{2}$$

where $J_n(\cdot)$ and $H_n^{(1)}(\cdot)$ are the first kind Bessel and Hankel functions, respectively, $\varphi(\omega)$ is the incident wave amplitude and ε_n is the Neumann factor ($\varepsilon_0 = 1$ and $\varepsilon_n = 2$ for $n \geq 1$). Coefficients A_n and B_n ($n = 0,1...,\infty$) were calculated by taking into account the continuity of displacement and stress at the cylinder boundary: $U_1 = U_2$ and $\sigma_{rz1} = \sigma_{rz2}$ at $r = R$ (Morse and Feshbach, 1953). Using displacements of Eq. (2) and calculating the normal stress at the boundary R, one obtains a system of two equations containing the infinite set of unknowns. The orthogonality property of trigonometric functions permits to separate, after some developments, the boundary conditions into an infinite set of systems of linear
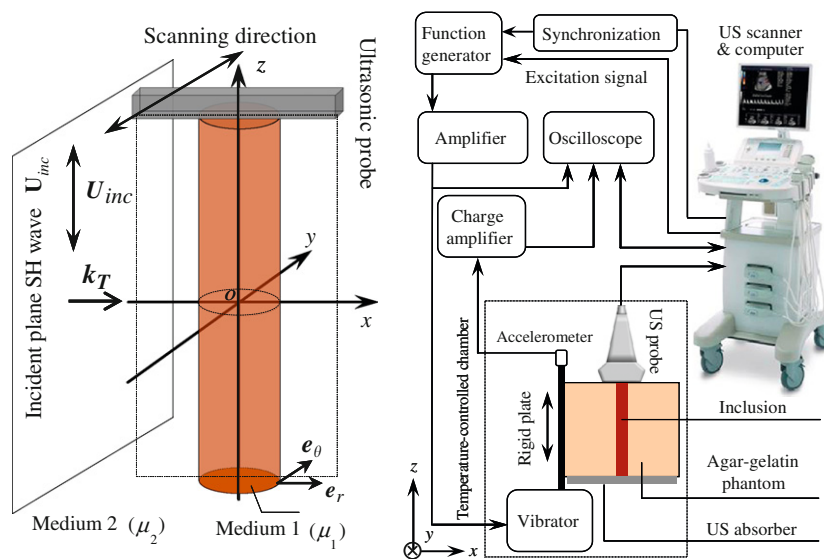
Fig. 1. (left) 3D representation of the plane SH wave scattered by the cylindrical heterogeneity and (right) experimental set-up used for measurements.

equations with respect to the order n

$$\mathbf{T}_n \begin{pmatrix} A_n \\ B_n \end{pmatrix} = \mathbf{b}_n \text{ with } r = R \text{ and } n = 0, \ldots, +\infty. \tag{3}$$

In Eq. (3), $\mathbf{T}_n$ and $\mathbf{b}_n$ are a matrix and a vector containing the nth order contribution of, respectively, scattered and incident fields to displacement and stress at the boundary. Knowing the geometrical and mechanical properties of the propagation heterogeneous medium, one can solve Eq. (3) for each order n (until a truncature order N). This leads to determine the searched coefficients and finally, from Eq. (2), the total stationary displacement field in both heterogeneity and propagation medium.

3. Experimental configuration

3.1. Phantom materials

First, to solve the forward problem, measurements on a first heterogeneous phantom was performed to compare experimentally observed resonance phenomena (eigenfrequencies, patterns of corresponding eigenmodes) with the theoretical ones. In a second time, two other heterogeneous phantoms were used to solve the inverse problem, i.e. to characterize the viscoelasticity of heterogeneities. All phantoms used in this study were designed to mimic blood clots.

For the first phantom, as depicted in Fig. 1, experiments were conducted on a surrounding material (medium 2) made of 4.0% porcine skin gelatin and 3.0% agar powder (Sigma Chemical, Saint-Louis, MO, USA) dissolved in distilled water and containing a very soft 5.0 mm radius circular cylinder (medium 1) made of 3.0% gelatin and 1.0% agar. To solve the forward problem (i.e., to validate the theoretical modeling), the viscoelastic properties of both agar–gelatin materials had to be measured before entering them into the model. The complex shear viscoelastic properties of agar-gelatin materials are governed by the Kelvin–Voigt model $\mu = \mu' + i\omega\eta$ (Catheline et al., 2004). This is in agreement with a previous study suggesting that the viscoelastic behavior of coagulated whole blood, in a frequency range of few hundred hertz, also follows a Kelvin–Voigt rheological model (Schmitt et al., 2007). Viscoelasticity of agar–gelatin materials were assessed, following a method described in Catheline et al. (2004), on two different cubic samples using harmonic plane shear waves with frequencies ranging between 50 and 400 Hz. We obtained $(2700 + 0.5i\omega)$ and $(17000 + 0.8i\omega)$ Pa for the complex viscoelastic shear coefficients μ_1 and μ_2, respectively, with relative errors (SD/mean) of $\pm 3.5\%$ for the elasticity and $\pm 13.0\%$ for the viscosity ($n \approx 50$ measures per sample).

Two other heterogeneous phantoms (indicated by letters A and B) were used to solve the inverse problem. Both of them were made of the same surrounding medium as the one used to validate the model (i.e., 4.0% porcine skin gelatin and 3.0% agar powder) and included 5.0 mm radius circular cylindrical inclusions. Phantom A contained a heterogeneity made of 3% gelatin and 1% agar, whereas the heterogeneity of phantom B was made of 3% gelatin and 2% agar. Viscoelastic parameters of these confined heterogeneities were labeled $\mu_1'^X$ and η_1^X (with $X=\{A,B\}$).

3.2. Shear wave generation and ultrasound acquisitions

SH waves were generated, as represented in Fig. 1, by a rigid vibrating plate connected to a vibrator (Brüel&Kjær, type 4810, Nærum, Denmark) and maintained in contact with the phantom. The vibrator displacement was powered by a function generator

(Agilent, model 33250A, Palo Alto, CA, USA) and measured by an accelerometer (Brüel&Kjær, type 4375, Nærum, Denmark). Radio frequency (RF) acoustic signals used to track vibrational motions within the phantom were acquired with a clinical 10 MHz array transducer (128 elements, 38.0 mm width) connected to a Sonix RP scanner (Ultrasonix Medical Corporation, Burnaby, BC, Canada) along an acquisition deep of 80.0 mm. Displacements of tissue speckles were calculated using a normalized cross-correlation algorithm applied on RF signals.

The high frame rate of the RF image acquisition system (3850 images per second) was obtained by using a shear wave gating method and a retrospective reconstruction strategy. The shear wave gating was developed similarly to the electrocardiogram-gated image acquisition strategy used by Chérin et al. (2006) and Pernot et al. (2007). In the present case, probe acquisitions over pairs of transducer elements (64 pairs) were synchronized with the beginning of the SH wave generation. Each pair was sequentially activated to generate ultrasound and receive echoes at a very high frame rate. Using this strategy, and for the probing depth of 80.0 mm, it was possible to increase the frame rate from about 20 Hz (when the 128 elements are simultaneously active in RF mode) to 3850 images per second. In post-processing, the retrospective reconstruction strategy consisted in loading stored RF signals, calculating displacements using a cross-correlation algorithm and assembling the successive calculated displacements over the different lines (corresponding to each pair of transducer elements) to build the four dimensional displacement matrix (width × depth × height × time).

4. Methods

First, with the objective of extracting the vibrational eigenfrequencies of the cylindrical heterogeneity, we measured the displacement spectrum produced by a set of harmonic SH incident waves at frequencies f ranging from 70 to 350 Hz (with $\Delta f = 0.5$ Hz). For this purpose, as represented in Figs. 1 and 2, an ultrasonic beam parallel to the z axis and crossing the plane (o, x, y) at M (-2.4, -1.15 mm), was used to measure out of plane displacements. A Fourier analysis, applied to the displacement temporal signals for each frequency, permitted to obtain the displacement amplitude of the heterogeneity at the excitation frequency and to construct the researched experimental spectrum. In order to compare the theory with experiments, the theoretical displacement spectrum was calculated, at position M, using the measured viscoelastic and geometrical properties of both media. For a realistic comparison, the incident SH wave used in simulations had an amplitude spectrum equal to the one measured by the accelerometer.

The second step of this study consisted in exciting, experimentally, the heterogeneous inclusion at the identified eigenfrequencies (e.g., f_1, f_2 and f_3 in Fig. 2b) to visualize the corresponding eigenmodes of vibration. The incident waves were composed of 20 sinusoidal oscillations with frequencies equal to those appearing in the resonance spectrum. The 3D scanning of the phantom was performed by sequentially translating, following the y axis, the ultrasonic probe to image 35 consecutive planes along a distance of 21.3 mm (Fig. 1). Since the scattering problem did not depend on the z coordinate, displacement fields were averaged, without filtering, following the elevational direction to get 2D displacement images in the temporal domain. The stationary displacement maps were obtained by first applying a Fourier transform to the temporally measured displacement fields and then, by extracting the complex displacement amplitude corresponding to the excitation frequency (i.e. the eigenfrequency). Theoretically, the displacement images corresponding to the eigenmodes were simulated, in the same spatial region, by the analytical model.

In order to explore the potential of SWIRE to characterize viscoelasticity of soft heterogeneities, we formulated and solved an inverse problem involving experimentally measured spectra, obtained as described above, and simulated ones. A minimization algorithm (nonlinear least-square problem solver using the Levenberg–Marquardt method to perform line search) solved the optimization problem expressed as

$$\underset{\mu', \eta}{Min} \sum_{i=1}^{N_{pt}} (U_1^{Exp}(f(i)) - U_1^{Sim}(\mu', \eta, f(i)))^2 \tag{4}$$

where U_1^{Exp} and U_1^{Sim} are the experimental and simulated displacement spectra into the heterogeneity, respectively, and $f(i)$ ($i=1,\ldots,N_{pt}$) are frequency samples of the spectra (N_{pt} was fixed to 200 samples centered onto f_1). In this equation, $\mu_1'^X$ and η_1^X (where $X=\{A,B\}$) are the searched parameters of the Voigt model governing

a

b
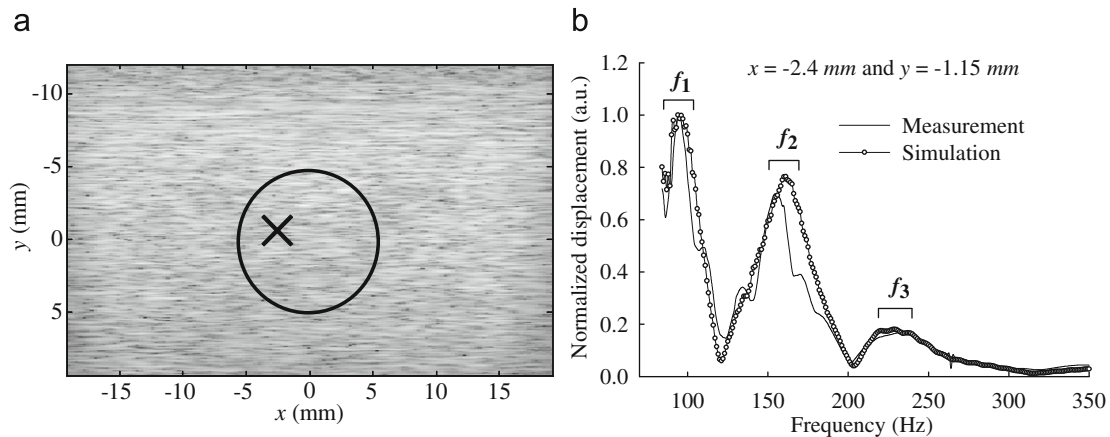
Fig. 2. (a) B-mode image of the experimental deep vein thrombosis phantom (for illustration purpose only, the ultrasound probe was moved to image the inclusion in cross-section, at $z=0$ mm). The cross represents the displacement spectrum measurement point M (-2.4, -1.15 mm). (b) Comparison of measured and simulated displacement spectra within the inclusion.

the viscoelastic behavior of the heterogeneities studied to solve the inverse problem.

In total, four acquisitions of resonance spectra were performed for each inclusion. After each, the ultrasonic probe was removed and repositioned to perform another measurement to evaluate the repeatability of the proposed method. For each acquisition, viscoelasticity of phantom heterogeneities A and B were evaluated, using the inverse problem of Eq. (4), on five experimental spectra calculated at different depths into the cylindrical inclusions to evaluate the spatial dependence of the method.

5. Results

5.1. Resonances and eigenmodes imaging (forward problem)

As shown in Fig. 2, three dominant frequencies clearly appear at $f_1=100$, $f_2=158$ and $f_3=230$ Hz in the measured displacement spectrum. The amplification of displacements at these frequencies is characteristic of resonance phenomena. Comparison of experimental and simulated spectra in Fig. 2 reveals a good correspondence of both curves, including the eigenfrequencies of the heterogeneity. The small differences in amplitude and frequency can be explained by the inter-sample variability on mechanical properties of materials 1 and 2. Nevertheless, one can conclude that the model is able to predict resonance frequencies and spectral response shapes that are directly related to the whole medium viscoelastic and geometrical properties.

The stationary displacement fields corresponding to the three identified and imaged eigenmodes are shown in three-dimensions in Fig. 3. It is noticeable that eigenmodes appear clearly and that a strong contrast exists between the inclusion displacement and that of the surrounding medium. To appreciate the add-on value of this new imaging modality, one may compare with the B-mode image of the whole medium, given in Fig. 2, which does not exhibit any echogenic contrast allowing to identify the inclusion. The resonance-mode images permit a clear segmentation of the inclusion boundary from displacement stationary images. This is particularly true for the first eigenmode, since this latter imposes to the whole cylinder an in-phase displacement along its axis. The second eigenmode has the particularity to split the inclusion in two equivalent parts vibrating in opposition of phase. The third eigenmode is characterized by the apparition of three vibrating regions: the inclusion center oscillates in opposition of phase with the two others. Fig. 4 shows, in two-dimensions, the good agreement between experimentally imaged eigenmodes and simulated ones, confirming again the validity of the proposed theoretical model of SH wave propagation.
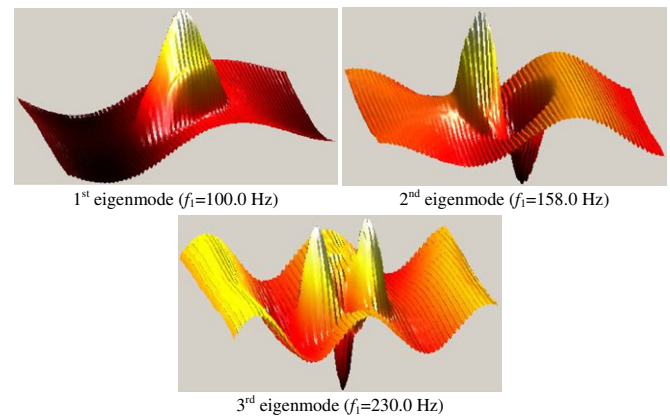
Fig. 3. 3D representation of the three experimentally measured eigenmodes of the cylindrical heterogeneity showing the out of plane normalized displacements.

5.2. Toward a viscoelasticity characterization method (inverse problem)

Results obtained by solving the inverse problem (4), shown in Fig. 5, exhibit a significant contrast between viscoelastic properties of heterogeneities A and B: $\mu'^A_1=(2174.2 \pm 32.5)$ compared with $\mu'^B_1=(3037.0 \pm 99.4)$ Pa, and $\eta^A_1=(0.49 \pm 0.03)$ versus $\eta^B_1=(0.79 \pm 0.09)$ Pa s. One can notice that the viscoelasticity of the agar–gelatin mixture is very sensitive to the concentration of its components. Indeed, in the present case, the addition of 1% agar resulted in elasticity and viscosity increases of 40% and 61%, respectively. The proposed characterization method also exhibited a good spatial reproducibility in elasticity (with a maximum relative error (SD/mean) of $\pm 2\%$) but more variability for the viscosity (maximum relative error of $\pm 17\%$). It is also noticeable that the proposed method was repeatable (from an acquisition series to another) with a maximum relative error of $\pm 3\%$ on elasticity and $\pm 11\%$ on viscosity.

6. Discussion

A new method, called shear wave induced resonance, for dynamic elastography imaging has been presented. Physically, resonance phenomena are explained by the convergence of shear wavefronts within the inclusion, since the inclusion was softer

1st vibration eigenmode corresponding to $f_1 = 100.0$ Hz

2nd vibration eigenmode corresponding to $f_2 = 158.0$ Hz

3rd vibration eigenmode corresponding to $f_3 = 230.0$ Hz
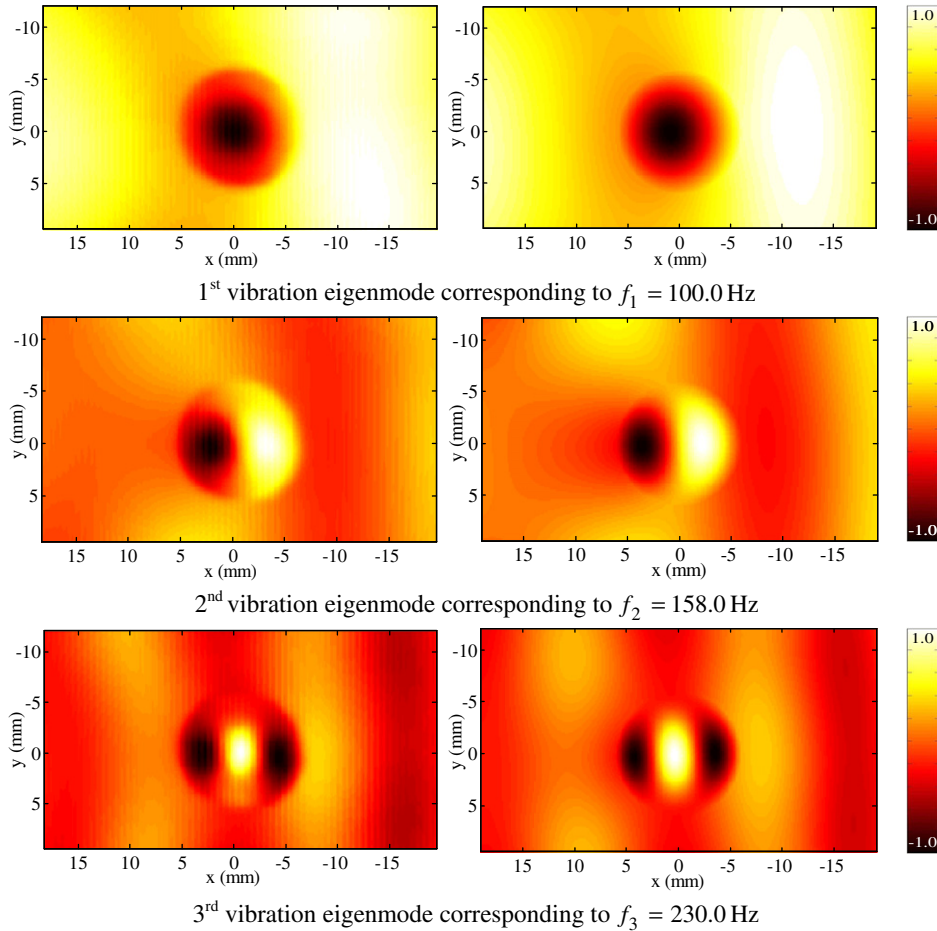
Fig. 4. Measured (left) and simulated (right) stationary normalized displacement fields of the three first eigenmodes.
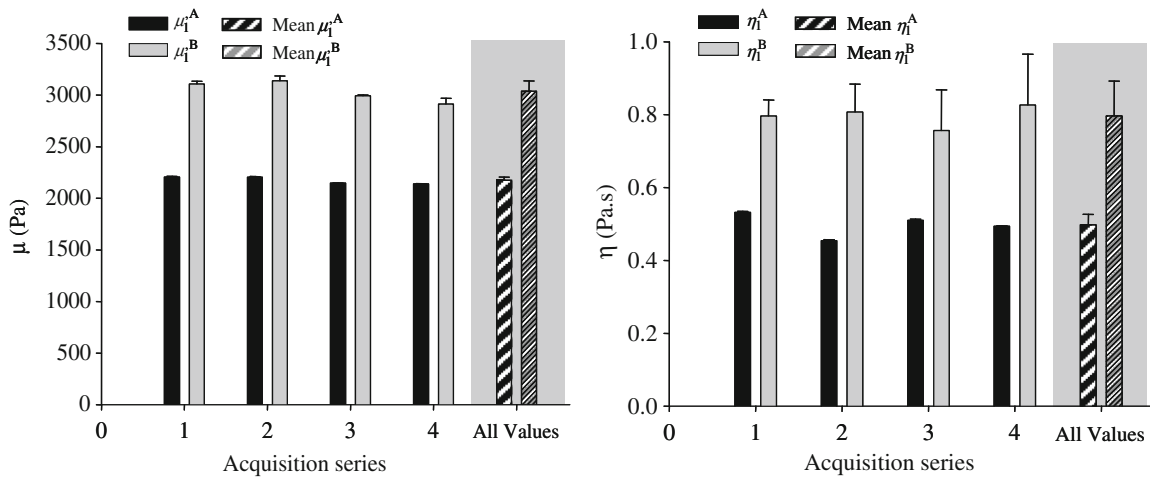
Fig. 5. Elasticity (μ'^A_1, μ'^B_1) and viscosity (η'^A_1, η'^B_1) values of agar–gelatin materials constituting heterogeneities of phantoms A and B obtained by solving the inverse problem for the four acquisitions. Results in gray area represent global mean values together with standard deviations.

than the surrounding medium. In addition, the absence of mode conversions affecting SH waves, which can be reasonably assumed with regards to the present experimental configuration (Achenbach, 1973; Auld, 1973), amplifies the observed resonance phenomenon. For certain incident wavelengths, corresponding to the eigenfrequencies and related to the inclusion geometry and viscoelasticity of both media, the constructive combination of the refracted wavefronts into the inclusion allowed the formation of standing waves and, consequently, the amplification of displacements. This mechanism is made possible by the viscoelastic contrast existing between the inclusion heterogeneity and that of the surrounding medium. At fixed mechanical properties, it is interesting to mention that the spectrum of resonance (i.e. both eigenfrequencies and eigenmodes) is shifted toward low frequencies when the heterogeneity dimension increases and, inversely, toward high frequencies when the diameter decreases.

The potential of SWIRE to discriminate mechanically heterogeneity from its background, since resonances are confined, has been shown. From a medical imaging point of view, in the absence of echogenicity contrast, as shown in the B-mode image of the whole phantom in Fig. 2, this advantage should allow to segment a different mechanical region directly from the eigenmode displacement images without calculating the elasticity map. Compared with static or standard dynamic elastography methods, the dynamical resonances enhance the displacement signal-to-noise ratio and could, under *in vivo* conditions, optimize the quality of elastography images, facilitate pathology segmentation and improve mechanical characterization. Future developments will generalize SWIRE to confined heterogeneities with more complex shapes like elliptical cross-section (as often encountered for partially collapsed veins), cylindrical wall containing a partial elliptical soft obstruction (to model the case of a partially occlusive thrombus), etc. In practical, the use of a transient excitation (with a large frequency bandwidth) should permit to extract, in a short acquisition time, at least the first resonance frequency. Moreover, one could note the flexibility of SWIRE since it could easily be coupled to other imaging modalities, like MRI elastography (Muthupillai et al., 1995) and supersonic shear imaging (Bercoff et al., 2004), to enhance the contrast of vascular thrombosis images and assess their viscoelasticity without any *a priori* on mechanical properties of underlying tissues. This last advantage is a key feature of the present method because it could permit to determine, in the explored frequency range, the viscoelastic behavior law (i.e. the rheological model) of vascular thrombosis under *in vivo* conditions. From a clinical point of view, the application of SWIRE to image and characterize vascular thrombosis has to be adapted to *in vivo* conditions. Indeed, one has to correct the biased measured displacements due to possible inclination of the ultrasound beam with respect to the pathology. In addition, since the shear wave source can possibly be inclined, mode conversions of elastic waves (between horizontally and vertically polarized shear waves) can affect the quality of resonances. Consequently, it is important to adapt the excitation and send a maximum of energy in the form of SH waves to take advantage of SWIRE in clinical applications.

Characterization results presented in this study show the sensitivity of the SWIRE-based inverse problem to discriminate heterogeneities with small contrast in viscoelasticity, with a satisfying precision and repeatability. In the light of results reported here concerning agar–gelatin mixtures, it is possible to conclude that SWIRE has the potential to characterize the viscoelasticity of soft materials. Moreover, since displacement resonance is measured over a relatively large frequency range and using an adapted inverse problem strategy, SWIRE could serve to determine the viscoelastic behavior law of biological tissues. Beyond these medical applications, SWIRE could also be adapted to propose an innovative rheology measurement instrument to characterize a wide range of soft and viscous materials currently encountered in industries like polymers, food, pharmacy, chemistry, hydrocarbons, etc.

Conflict of interest statement

None of the authors in this work has conflict of interests with other people and organizations.

Acknowledgments

References

Achenbach, J.D., 1973. Wave Propagation in Elastic Solids. North-Holland, Amsterdam.

Auld, B.A., 1973. Acoustic Fields and Waves in Solids.. John Wiley & Sons, New York.

Bercoff, J., Tanter, M., Fink, M., 2004. Sonic boom in soft materials: the elastic Cerenkov effect. Applied Physics Letters 84, 2202–2204.

Biwa, S., Yamamoto, S., Kobayashi, F., Ohno, N., 2004. Computational multiple scattering analysis for shear wave propagation in unidirectional composites. International Journal of Solids and Structures 41 (2), 435–457.

Burghardt, W.R., Goldstick, T.K., Leneschmidt, J., Kempka, K., 1995. Nonlinear viscoelasticity and the thromblelastograph: 1. studies on bovine plasma clots. Biorheology 32, 621–630.

Catheline, S., Gennisson, J.-L., Delon, G., Fink, M., Sinkus, R., Abouelkaram, S., Culioli, J., 2004. Measurement of viscoelastic properties of homogeneous soft solid using transient elastography: an inverse problem approach. The Journal of the Acoustical Society of America 116, 3734–3741.

Chérin, E., Williams, R., Needles, A., Liu, G., White, C., Brown, A.S., Zhou, Y.-Q., Foster, F.S., 2006. Ultrafast frame rate retrospective ultrasound microimaging and blood flow visualization in mice *in vivo*. Ultrasound in Medicine and Biology 32, 683–691.

Eisencher, A., Schweg-Toffler, E., Pelletier, G., Jacquemard, P., 1983. La palpation échographique rythmée: echosismographie. Journal of Radiology 64, 255–261.

Emelianov, S.Y., Chen, X., O'Donnell, M., Knipp, B., Myers, D., Wakefield, T.W., Rubin, J.M., 2002. Triplex ultrasound: elasticity imaging to age deep venous thrombosis. Ultrasound in Medicine and Biology 28, 757–767.

Evans, P.A., Hawkins, K., Lawrence, M., Williams, R.L., Barrow, M.S., Thirumalai, N., Williams, P.R., 2008. Rheometry and associated techniques for blood coagulation studies. Medical Engineering & Physics 30, 671–679.

Fatemi, M., Greenleaf, J.F., 1998. Ultrasound-stimulated vibro-acoustic spectrography. Science 3 (280), 82–85.

Flax, L., Dragonette, L.R., Überall, H., 1978. Theory of elastic resonance excitation by sound scattering. The Journal of the Acoustical Society of America 63, 723–731.

Greenleaf, J.F., Fatemi, M., Insana, M., 2003. Selected methods for imaging elastic properties of biological tissues. Annual Review of Biomedical Engineering 5, 57–78.

Hadj Henni, A., Schmitt, C., Cloutier, G., 2008. Three-dimensional transient and harmonic shear-wave scattering by a soft cylinder for dynamic vascular elastography. The Journal of the Acoustical Society of America 124, 2394–2405.

Kaibara, M., 1996. Rheology of blood coagulation. Biorheology 33, 101–117.

Krouskop, T.A., Dougherty, D.R., Vinson, F.S., 1987. A pulsed Doppler ultrasonic system for making noninvasive measurements of the mechanical properties of soft tissue. Journal of Rehabilitation Research and Development 24, 1–8.

Morse, P.M., Feshbach, H., 1953. Methods of Theoretical Physics. McGraw-Hill, New York, p. 1376, (Chapter 11.2).

Muthupillai, R., Lomas, D.J., Rossman, P.J., Greenleaf, J.F., Manduca, A., Ehman, R.L., 1995. Magnetic resonance elastography by direct visualization of propagating acoustic strain waves. Science 269, 1854–1857.

Palmeri, M.L., Sharma, A.C., Bouchard, R.R., Nightingale, R.W., Nightingale, K.R., 2005. A finite-element method model of soft tissue response to impulsive acoustic radiation force. IEEE transactions on Ultrasonics, Ferroelectrics, and Frequency Control 52, 1699–1712.

Papazoglou, S., Xu, C., Hamhaber, U., Siebert, E., Bohner, G., Klingebiel, R., Braun, J., Sack, I., 2009. Scatter-based magnetic resonance elastography. Physics in Medicine and Biology 54, 2229–2241.

Parker, K.J., Huang, S.R., Musulin, R.A., Lerner, R.M., 1990. Tissue response to mechanical vibrations for "sonoelasticity imaging". Ultrasound in Medicine & Biology 16, 241–246.

Parker, K.J., Lerner, R.M., 1992. Sonoelasticity of organs: shear waves ring a bell. Journal of Ultrasound in Medicine 11, 387–392.

Pernot, M., Fujikura, K., Fung-Kee-Fung, S.D., Konofagou, E., 2007. ECGgated, mechanical and electromechanical wave imaging of cardiovascular tissues *in vivo*. Ultrasound in Medicine and Biology 33, 1075–1085.

Rubin, J.M., Aglyamov, S.R., Wakefield, T.W., O'Donnell, M., Emelianov, S.Y., 2003. Clinical application of sonographic elasticity imaging for aging of deep venous thrombosis: preliminary findings. Journal of Ultrasound in Medicine 22, 443–448.

Ryan, E.A., Mockros, L.F., Weise, J.W., Lorand, L., 1999. Structural origins of fibrin clot rheology. Biophysical Journal 77, 2813–2826.

Schmitt, C., Hadj Henni, A., Cloutier, G., 2007. Characterization of timevarying mechanical viscoelastic parameters of mimicking deep vein thrombi with 2D dynamic elastography, Proceedings of the IEEE International Ultrasonics Symposium.

Shah, J.V., Janmey, P.A., 1997. Strain hardening of fibrin gels and plasma clots. Rheologica Acta **36**, 262–268.

Williams, P.R., Hawkins, K., Wright, C., Evans, A., Simpkin, H., Barrow, M.S., Williams, R.L., 2006. Rheometrical and computational studies of blood viscoelasticity during coagulation. Clinical Hemorheology and Microcirculation 35, 123–127.